Experimental Observations and Integrity Monitor Applications of LAAS IMLA Carrier Phase Measurements

L. Gratton, S. Khanafseh, B. Pervan, *Illinois Institute of Technology*
S. Pullen, *Stanford University*
J. Warburton, *William J. Hughes FAA Technical Center*

ABSTRACT

This paper evaluates the integrity performance of carrier phase measurement based monitors for the Local Area Augmentation System Ground Facility. It shows the experimental verification for the type A1 ephemeris threat monitor (after-maneuver validation) and initial results for an ionospheric threat monitor for a static storm. It starts by describing in detail the carrier phase performance of the Integrated Multipath Limiting Antennas (IMLA's), including an assessment of differential phase pattern variations with respect to azimuth and elevation. It also defines the mathematical model developed for differential phase variation, explains its use in precise antenna calibration, and demonstrates that the resulting IMLA double difference carrier phase errors have a standard deviation of less than 3 mm. Finally, the calibrated double difference carrier phase measurements are used toward the detection of the ephemeris and ionospheric front anomalies. The integrity performance of the LGF SIS monitor functions is quantified analytically and by simulation, and verified experimentally by deliberately injecting failures into the broadcast ephemeris or the raw LTP data.

INTRODUCTION

The Local Area Augmentation System (LAAS) will include multiple, spatially separated Integrated Multipath Limiting Antennas (IMLA's) at each LAAS Ground Facility (LGF). The primary reason for the use of multiple reference receivers and antennas at the LGF is to provide a means for detection and isolation of a failed receiver and also to allow for a net reduction in ranging error by averaging measurements for a given satellite. Spatial separation of the reference antennas is implemented to ensure sufficient decorrelation of multipath errors so that the averaging process is effective. However, a generally unrecognized benefit of such antenna separation is that differential carrier phase measurements across the antennas baselines can be used to detect and isolate certain signal-in-space (SIS) failures and anomalies that are hazardous to LAAS. Two major classes of anomalies that fall into this category are satellite ephemeris failures and ionospheric storms. In this paper we investigate the use of highly precise IMLA differential carrier phase measurements for these critical LGF SIS integrity monitor applications.

Two basic types of orbit ephemeris threat are recognized: Type A, where the broadcast ephemeris data is erroneous following a satellite maneuver, and Type B, where the broadcast ephemeris data is erroneous, but no satellite maneuvers are involved. Type B failures are easier to detect because anomalies can be identified by comparison with prior validated broadcast ephemerides. In contrast, prior ephemerides are of no use in the detection of Type-A failures because of the intervening maneuver. In this case, the necessary LGF-based ephemeris fault detection must rely on LGF measurements directly [1]. A proposed method toward this purpose is to use double difference carrier phase measurements from the known baselines between the IMLA antennas to directly observe the effect of an ephemeris anomaly. However, the effectiveness of these observations for detection is directly related to the baseline lengths and the quality (standard deviation) of the differential carrier phase measurement error. Keeping the necessary distance between the antennas relatively small is very important as the airports have physical constraints regarding their siting. Covariance analysis results have shown that this approach is realizable for baselines less than 200 m long, but only if the standard deviation of the double difference carrier measurement error is 5 mm or lower [2].

Ionospheric storms can also produce hazardous conditions for LAAS navigation. Of greatest concern in this regard are sharp ionospheric fronts, which can be either stationary or moving relative to the LGF. Moving fronts can be detected by monitoring the code-carrier divergence

over time for each satellite at the LGF. However, slowly moving (nearly stationary) fronts can be very difficult to detect with such a monitor because the observations of divergence will change very slowly. In contrast, a baseline carrier phase monitor can potentially detect many of these fronts because it samples the change in ionospheric delay over distance, not time. However, the ultimate performance of such a monitor is also directly influenced by standard deviation of the nominal differential carrier phase measurement error. In the case of the ephemeris monitor, covariance analysis in [1] shows that it is essential that the carrier phase error standard deviation be less than 5mm for the double difference measurements.

The IMLA was specifically designed to meet the LAAS LGF requirements of accuracy, availability and integrity, but the uses envisioned here for the IMLA pose a new challenge because the required precision for carrier phase measurements is not necessary for the nominal fault-free LAAS functionality and was not a specific requirement in the design of these antennas. However, the exceptional theoretical noise and multipath performance of the IMLA suggests that such carrier phase precision should be achievable in principle.

The IMLA consists of two combined antennas: the Multipath Limiting Antenna (MLA) and the High Zenith Antenna (HZA). The MLA is a 14-element dipole array antenna that covers elevation angles of 0-35 degrees; it is resistant to terrestrial interference sources and meets the required signal-noise ratio at low elevations. The HZA is a cross-V-dipole antenna that covers elevation angles above 35 degrees and meets the LGF stringent requirements regarding signal-noise ratio and multipath rejection. Thornberg, et al. [3] showed that IMLA achieved ground multipath rejection on the order of 35dB throughout the entire hemispherical coverage volume. This suggests that the carrier phase precision needed for LGF monitors should be achievable, but the behavior of the antennas has not been studied in detail at the millimeter level before. Of particular importance in this regard are the potential variations in phase patterns between antennas. To study the measurements experimentally, IMLA data collected at the LAAS Test Prototype (LTP) facility at the William J. Hughes FAA Technical Center in Atlantic City, New Jersey was used.

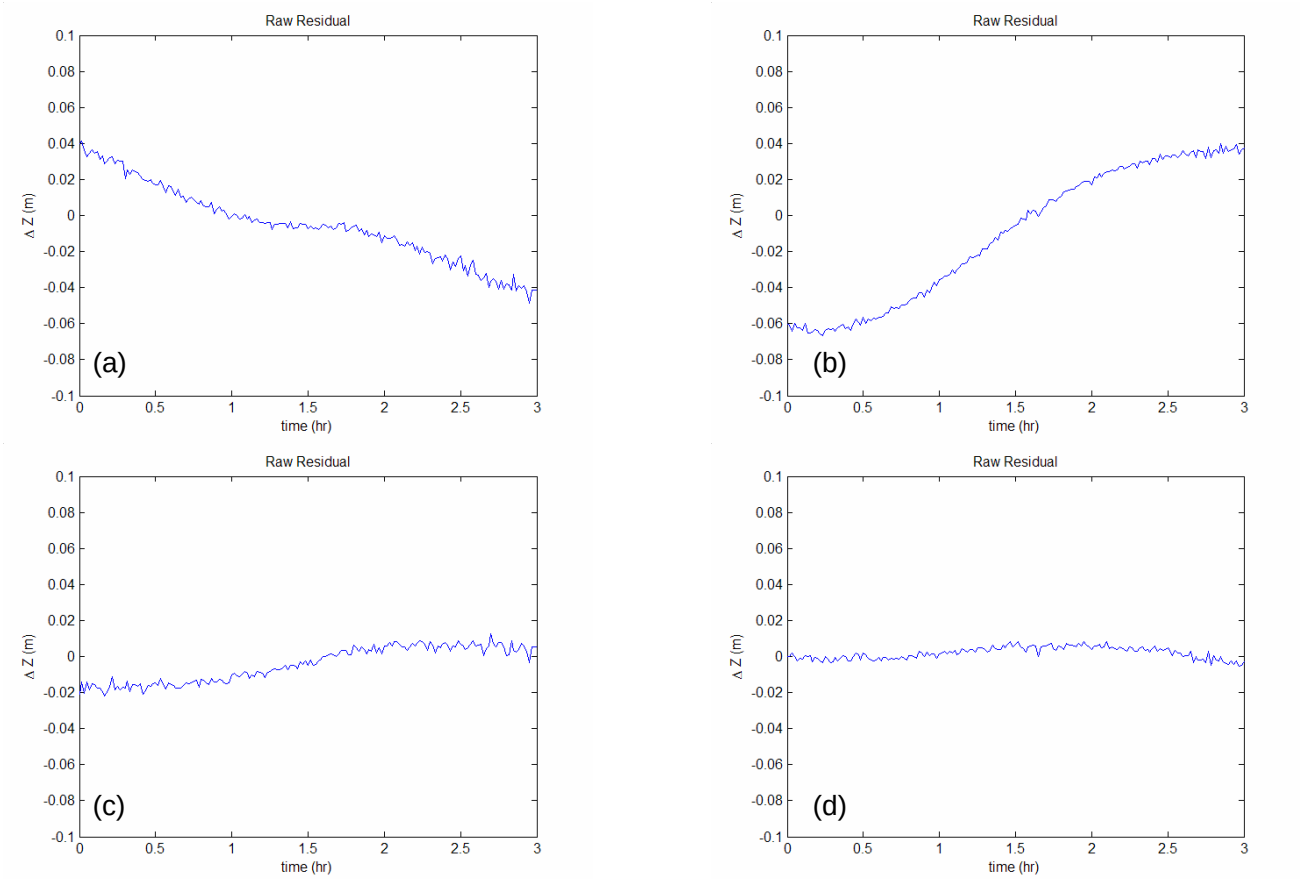

Figure 1: Double difference carrier phase residuals. (a) AB baseline PRNs 27 & 31. (b) AB baseline PRNs 10 & 24. (c) CB baseline PRNs 27 & 31. (d) CB baseline PRNs 10 &24.

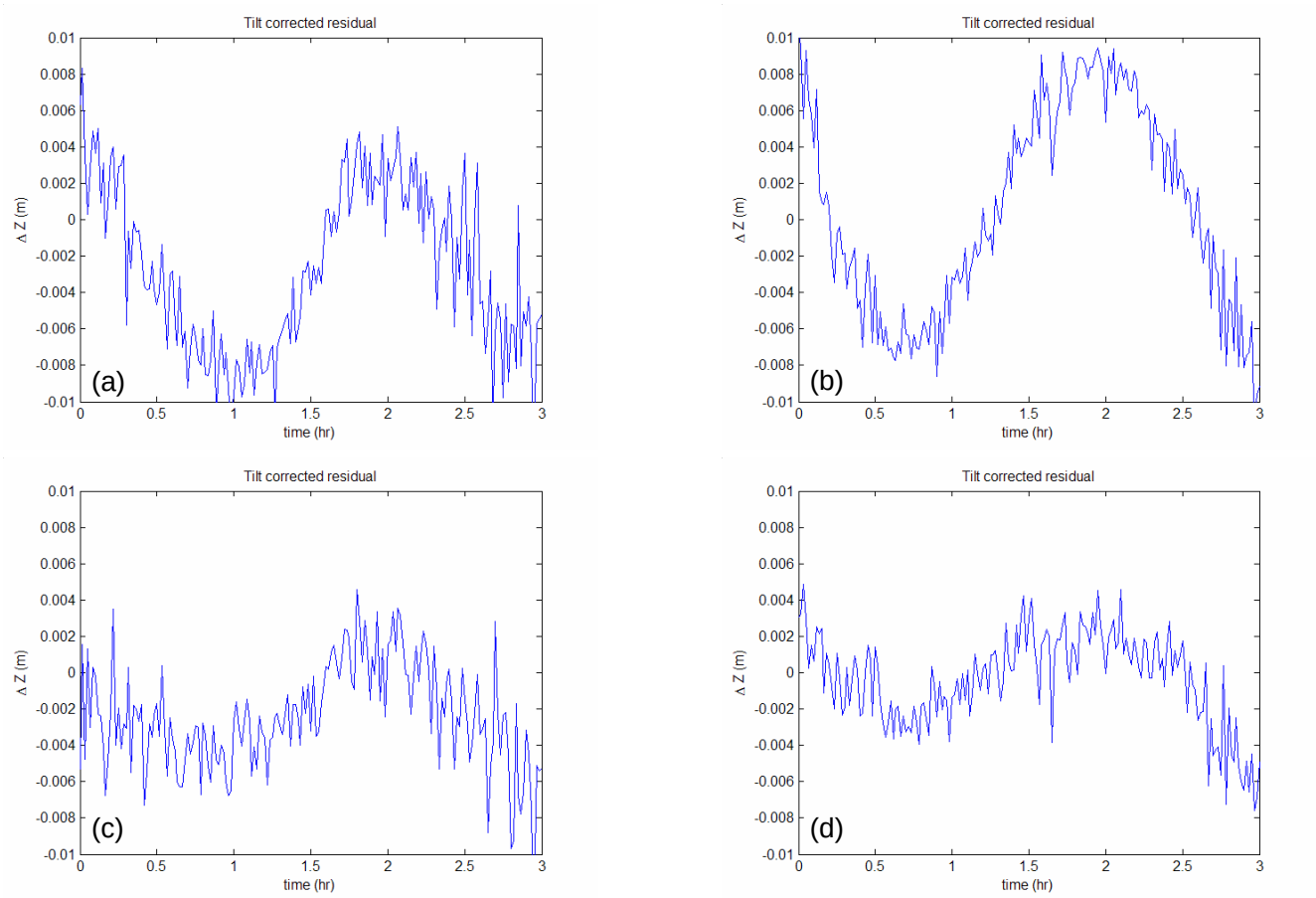

Figure 2: Tilt corrected double difference carrier phase residuals. (a) AB baseline PRNs 27 & 31. (b) AB baseline PRNs 10 & 24. (c) CB baseline PRNs 27 & 31. (d) CB baseline PRNs 10 &24.

LTP IMLA CARRIER PHASE ANALYSIS

The raw data from the LTP site was collected using four IMLA antennas (one HZA and one MLA each). In this paper, only the first three antennas, (marked A, B and C) are used. The HZA double difference carrier phase data is discussed first. As shown in Figure 1 non-random residual errors are much larger and at lower frequency than what can be caused by multipath and thermal noise variations. Furthermore, the residual ramp and wavy behavior shows day-to-day repeatability indicating that the source of the effect is a systematic difference in the phase patterns between antennas. The ramps have been easily corrected by surveying the baseline vector for 24 hours. New survey vectors were generated for baselines AB and BC. The difference might be explained by a tilt in the antenna posts. After using the "tilt corrected baseline" (Figure 2), the residual behavior does not show centimeter level ramp patterns but instead, a millimeter level wavy pattern appeared. This pattern is also day-to-day repeatable and could not be ignored because of its effect on increasing the standard deviation of the double difference residual.

SPERICAL HARMONICS MODEL

After studying the wavy structure for different satellite pairs, it was concluded that this pattern is related to the azimuth and elevation of the satellites. Therefore, a model that can represent the phase pattern variation effect of azimuth and elevation on the residuals is pursued. The spherical harmonics function (Legendre's trigonometric polynomial series of order **n** and degree **m** (Equation 1)) can be useful in this case.

$$U(\theta,\phi) = \sum_{n=0} J_n P_{n0}(\cos\theta) + \sum_{n=1}\sum_{m=1}^{n} [C_{nm}\cos m\phi + S_{nm}\sin m\phi] P_{nm}(\cos\theta) \quad (1)$$

where,

J_n, C_{nm} and S_{nm}: spherical coefficients,
θ: zenith angle
ϕ: azimuth angle
P_{nm}: Legendre' polynomial of order n, degree m.

The model used to calibrate the antennas computes the carrier phase measurement difference between two

antennas (u and r) to the same satellite (k) and adds the spherical harmonics term as a function of the satellite angles (θ^k and ϕ^k) (Equation 2).

$$\begin{aligned}\lambda\Phi_{ur}^{k} &= \rho_{ur}^{k} + c\cdot\delta t_{ur} + \lambda N_{ur}^{k} + U_{ur}\left(\theta^k,\phi^k\right) + \varepsilon'^{k}_{ur} \\ &= \rho_{ur}^{k} + c\cdot\delta t_{ur} + \lambda N_{ur}^{k} + \sum_{n=0} J_{ur,n} P_{n0}\left(\cos\theta^k\right) + \\ &\sum_{n=1}^{n}\sum_{m=1}^{n}\left[C_{ur,nm}\cos m\phi^k + S_{ur,nm}\sin m\phi^k\right]P_{nm}(\cos\theta^k) \\ &+ \varepsilon'^{k}_{ur}\end{aligned} \tag{2}$$

where,

Φ^k_{ur}: difference of carrier phase measurement between u and r for satellite k.
λ: wave length
ρ: user satellite distance
c: speed of light
δt: receiver clock bias
N: integer ambiguity; and

$$P_{nm}(x) = 2^{-n}\left(1-x^2\right)^{m/2} \sum_{k=0}^{l}(-1)^k \frac{(2n-2k)!}{k!(n-k)!(n-m-2k)!}x^{n-m-2k}$$

By writing the same formula for another satellite (l) we get:

$$\begin{aligned}\lambda\Phi_{ur}^{l} &= \rho_{ur}^{l} + c\cdot\delta t_{ur} + \lambda N_{ur}^{l} + \sum_{n=0} J_{ur,n} P_{n0}\left(\cos\theta^l\right) + \\ &\sum_{n=1}^{n}\sum_{m=1}^{n}\left[C_{ur,nm}\cos m\phi^l + S_{ur,nm}\sin m\phi^l\right]P_{nm}(\cos\theta^l) \\ &+ \varepsilon'^{l}_{ur}\end{aligned} \tag{3}$$

Since the spherical coefficients (J_n, C_{nm} and S_{nm}) are characteristic of the antennas and not the satellite angles, these coefficients can be considered common factors ($K_{ur,nm}$) when taking the double difference (between equation 2 and equation 3),

$$\begin{aligned}\lambda\Phi_{ur}^{kl} &= -\left(e_r^k - e_r^l\right)^T x_{ur} + \lambda N_{ur}^{kl} + \\ &\sum_{n=0} J_{ur,n}\left[P_{n0}\left(\cos\theta^k\right) - P_{n0}\left(\cos\theta^l\right)\right] + \\ &\sum_{n=1}^{n}\sum_{m=1}^{n} C_{ur,nm}\left(\cos m\phi^k - \cos m\phi^l\right)\left[P_{nm}(\cos\theta^k) - P_{nm}(\cos\theta^l)\right] \\ &+ \sum_{n=1}^{n}\sum_{m=1}^{n} S_{ur,nm}\left(\sin m\phi^k - \sin m\phi^l\right)\left[P_{nm}(\cos\theta^k) - P_{nm}(\cos\theta^l)\right] \\ &+ \varepsilon'^{l}_{ur}\end{aligned}$$

which can be expressed in a simplified form as:

$$\begin{aligned}\lambda\Phi_{ur}^{kl} &= -\left(e_r^k - e_r^l\right)^T x_{ur} + \lambda N_{ur}^{kl} + \\ &\sum_{n=1}^{n}\sum_{m=1}^{n}\Delta P_{nm}\left(\theta^k,\theta^l,\phi^k,\phi^l\right)\cdot K_{ur,nm} + \varepsilon'^{l}_{ur}\end{aligned} \tag{4}$$

It should be mentioned that the first three components of the series (1st order) are the same as the baseline vector correction done earlier. Thus, these three components were omitted from the series. Finally, Equation 4 can be rewritten in a vector form as shown in Equation 5 and the coefficients ($K_{ur,nm}$) can be estimated by using a Kalman filter for all satellites in view in 24 hours.

$$\begin{aligned}&\left[\lambda\Phi_{ur}^{kl} + \left(e_r^k - e_r^l\right)^T x_{ur} - \lambda N_{ur}^{kl}\right] = \\ &\left[\Delta P_{nm}\left(\theta^k,\theta^l,\phi^k,\phi^l\right)\right]\cdot\left[K_{ur,nm}\right] + \varepsilon'^{l}_{ur}\end{aligned} \tag{5}$$

After trying different orders (n), it was found that an 8th order (n = 8) model is sufficient to reduce the wave amplitude (get the required value of sigma) and higher order models do not show significant improvements. The corrected residuals using the spherical harmonics model for both baselines are shown in Figure 3. While small amplitude wavy structure might exist in some cases, the standard deviation of the residual was always found to be less than 3mm. This wavy structure can be explained by the fact that the spherical harmonics basis functions are orthogonal in the domain ($0< \theta < 90$ and $0< \phi < 360$). But for the HZA, the data domain is $0< \theta < 65$ and $0< \phi < 360$, which might affect the orthogonality of the basis function and in turn affect the efficiency of the spherical harmonics model for this specific case.

SPHERICAL HARMONICS MODEL VALIDATION

The coefficients estimated earlier ($K_{ur,nm}$) can be used to construct a double difference correction map of the sky (Figure 4). The sky map is normalized against an arbitrary reference point that is chosen to be the 90-degree elevation point. It can be seen that the sky maps are not symmetric and not even analogous for both baselines, which again suggests that the cause is individual phase center variations of these antennas. These sky maps help to understand the phase patterns of these antennas. In addition, given the azimuth and elevation angles of any two satellites, this map can be used to get the amount of correction to be added to the double difference carrier phase residual. The sky map and the estimated coefficients are site dependent and the results shown in this work are only for the LTP site. If this calibration is performed in any other airport or facility, or the antennas are different, new coefficients must be estimated.

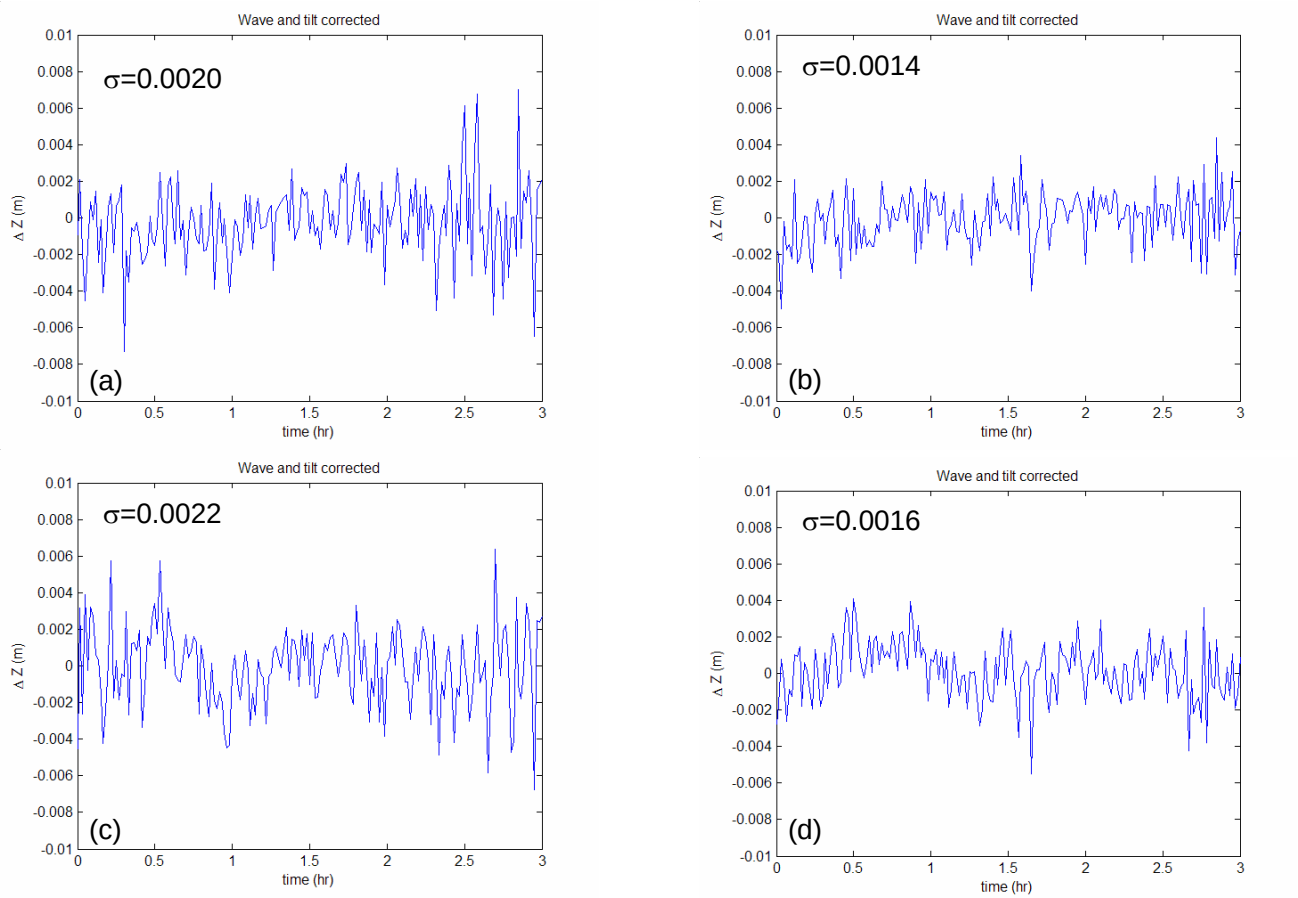

Figure 3: Tilt and wave corrected double difference carrier phase residuals. (a) AB baseline PRNs 27 & 31. (b) AB baseline PRNs 10 & 24. (c) CB baseline PRNs 27 & 31. (d) CB baseline PRNs 10 &24.

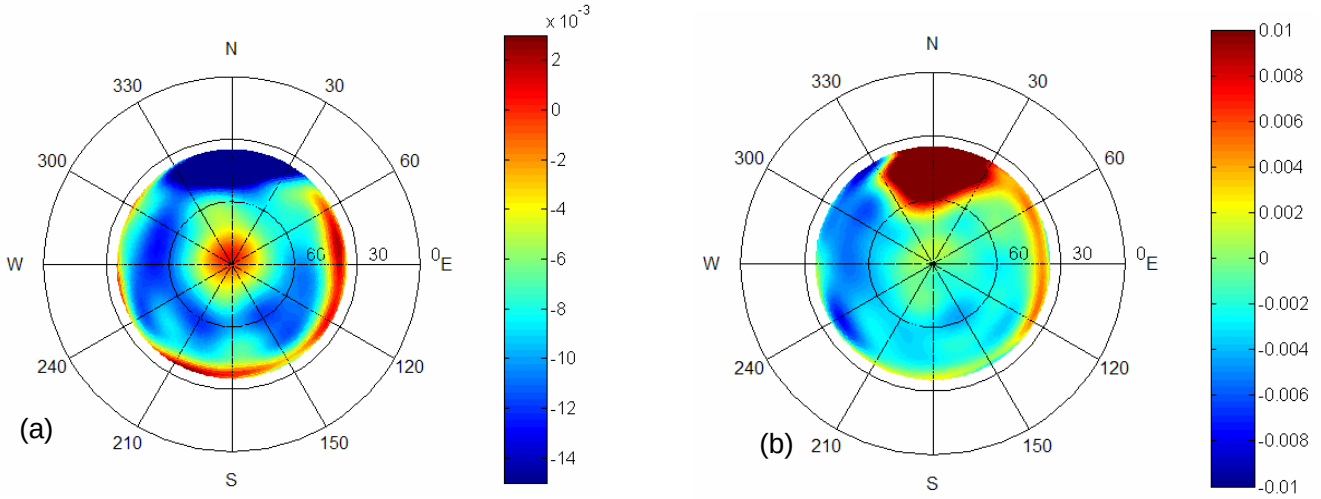

Figure 4: Sky map of the double difference residual correction. (a) AB baseline. (b) CB baseline.

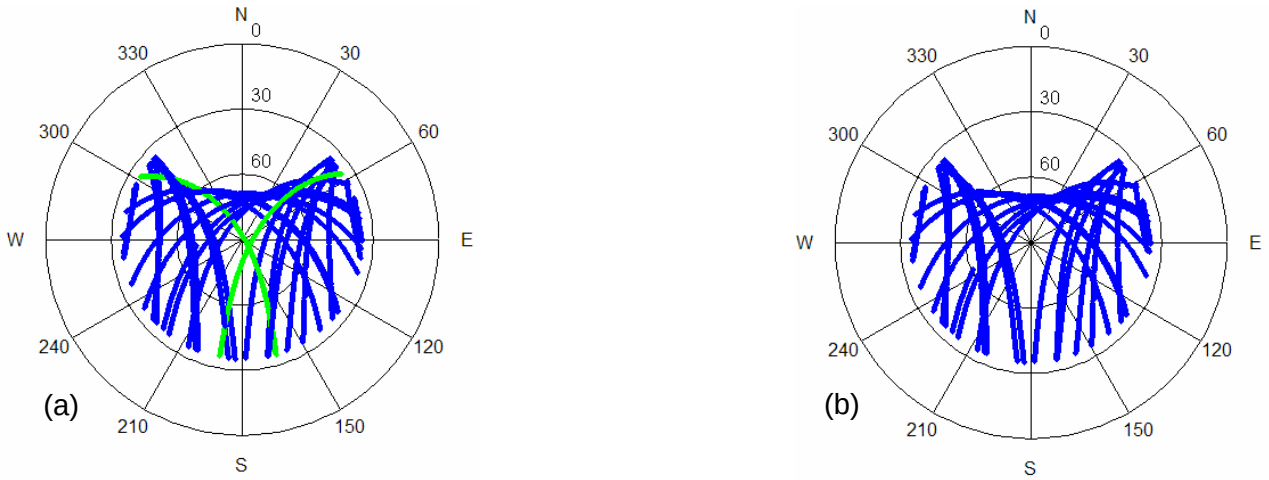

Figure 5: polar plot of satellite paths used in 24 hour analysis. (a) "full constellation". (b) "artificial constellation" (PRN's 22, 28 and 31 "green" in (a) were removed).

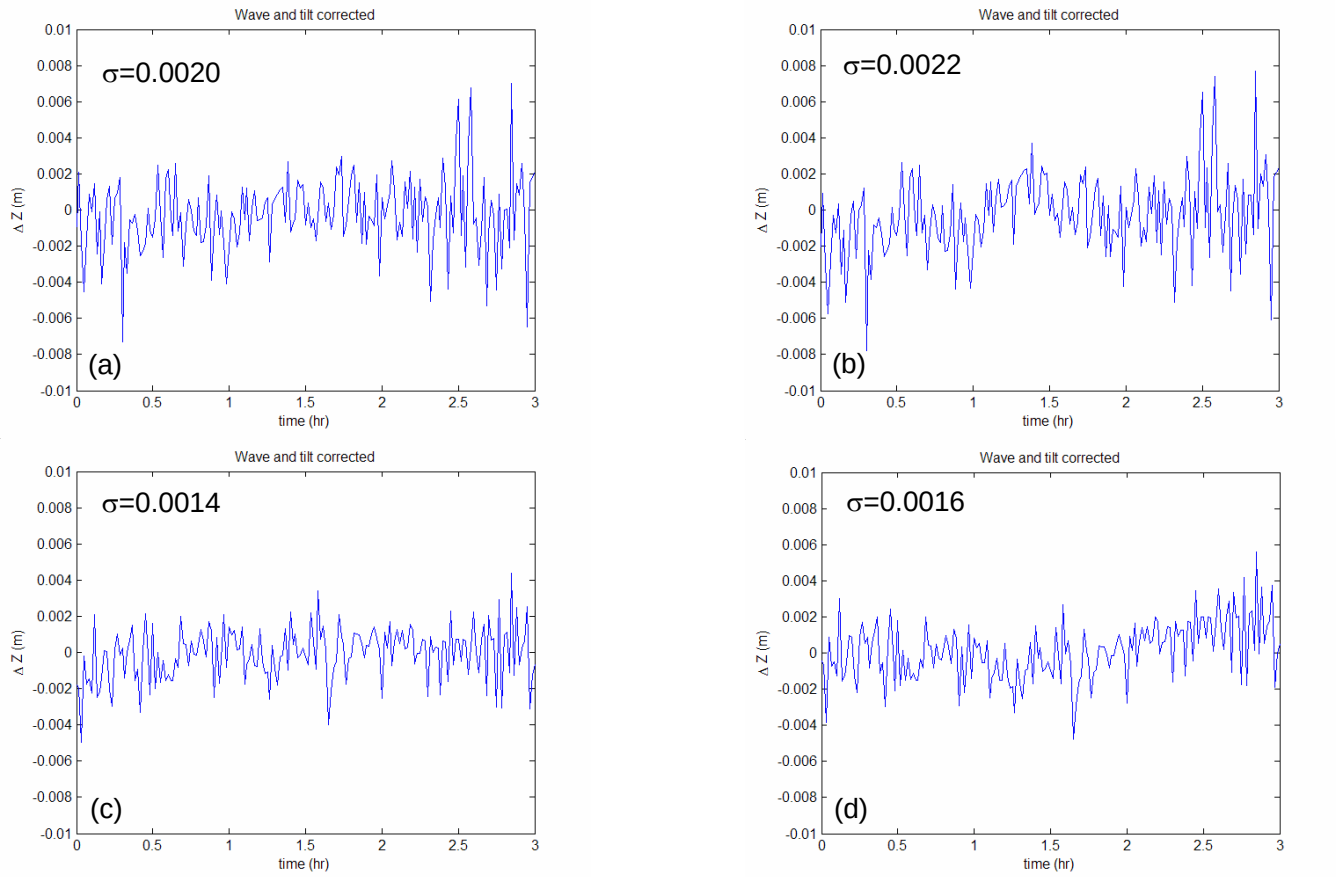

Figure 6: Tilt and wave corrected double difference carrier phase residuals for AB baseline. (a) PRNs 27 & 31 with "full constellation". (b) PRNs 27 & 31 with "artificial constellation". (c) PRNs 10 & 24 with "full constellation". (b) PRNs 10 & 24 with "artificial constellation".

The spherical harmonics model should be valid for changes in constellation (like adding a new satellite or orbit changes by time) allowing it to be used directly without modifications. In order to test the model's validity for changes in constellation, an "artificial constellation" is made by deliberately removing three satellites (PRN 22, 28 and 31 in green traces in Figure 5) from the previous "full constellation" used. Notice that

removing these three satellites creates a gap in the sky. The artificial constellation is used to generate the spherical coefficients ($K_{ur,nm}$) and to calculate the residuals for the 3 satellites that were removed. The results are then compared to the ones obtained using the "full constellation" (Figure 6 and 7), which mimic the case of adding these three satellites to the constellation. The results of this validation shown in Figures 6 and 7 illustrate that sigma is still less than 3 mm and is only 0.2 mm higher for the reduced constellation, showing the model's robustness for changes in constellation.

MLA CALIBRATION

One fundamental difference between the MLA and HZA antennas is that the vertical location of the MLA phase center depends on the azimuth and elevation angle of the satellite and that this variation can reach up to 10 cm. If the same analysis of surveying the MLA baseline is to be used for the HZA, this variation will cause a problem in estimating a static baseline fix. Therefore, surveying the baseline vector to get the tilt amount in the MLA antennas is irrelevant. The uncorrected HZA baseline vector will be used instead, using all spherical harmonics coefficients (including the first 3) to compensate for these variations. Since the MLA data elevation angles range from 5 to 35 degrees, the measurements have shorter passes than the HZA. Accordingly, it is even harder to perfectly fit the residuals to the spherical harmonics because the basis functions are not perfectly orthogonal in the MLA domain ($65< \theta < 85$ and $0< \phi < 360$). This can be clearly seen in Figure 8 where small ramps and/or waves can be observed. However, standard deviations of the double difference residual are generally below 3 mm.

After being subject to the calibration procedure shown above, the measurement data from the HZA and MLA antennas is suitable to be used in detecting and isolating certain SIS failures and anomalies, as the standard deviation has been reduced to a level below 3 mm and the waves have been largely removed and explained. In the following sections, monitors for satellite ephemeris failures and ionospheric front anomalies will be studied using the LTP calibrated data.

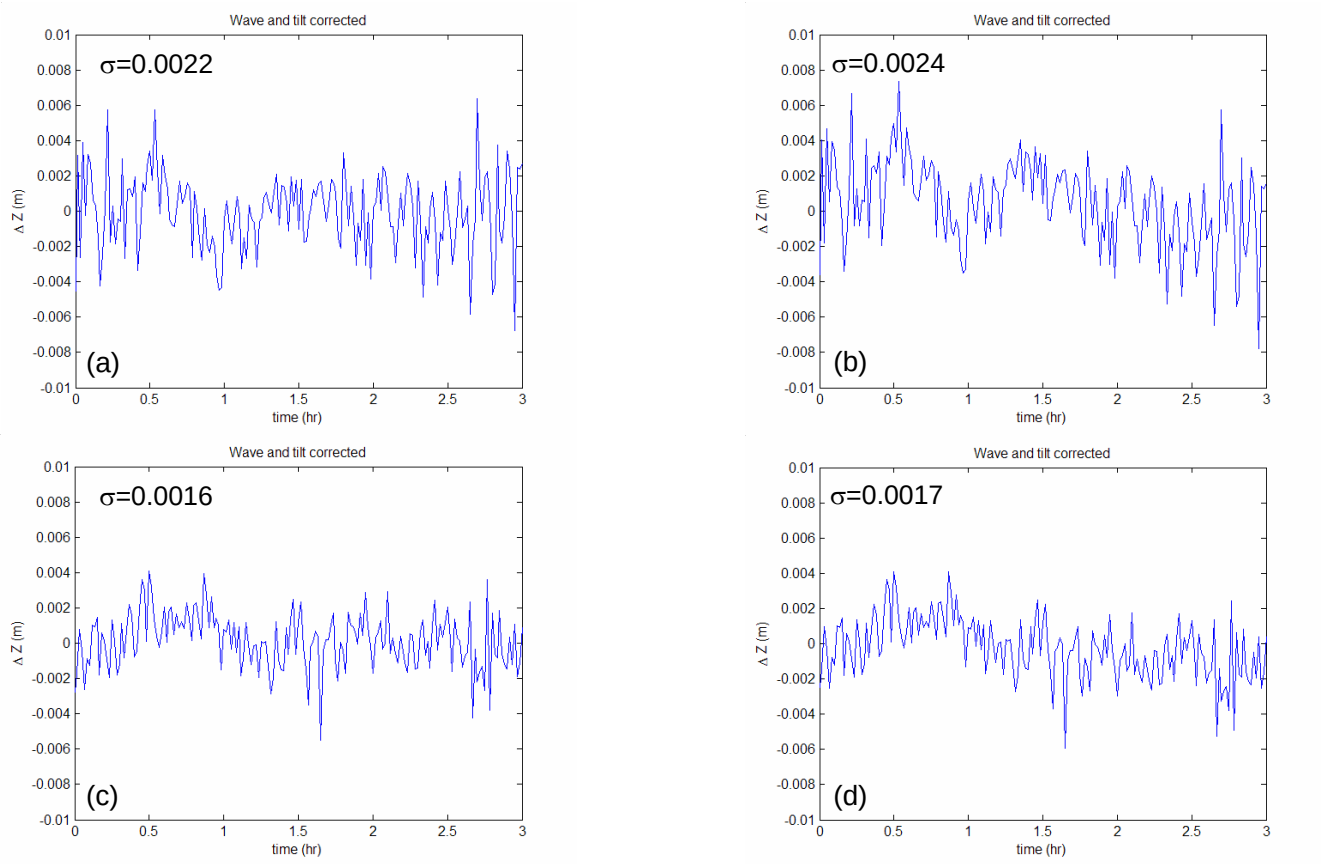

Figure 7: Tilt and wave corrected double difference carrier phase residuals for CB baseline. (a) PRNs 27 & 31 with full constellation. (b) PRNs 27 & 31 with three satellites removed. (c) PRNs 10 & 24 with full constellation. (b) PRNs 10 & 24 with three satellites removed.

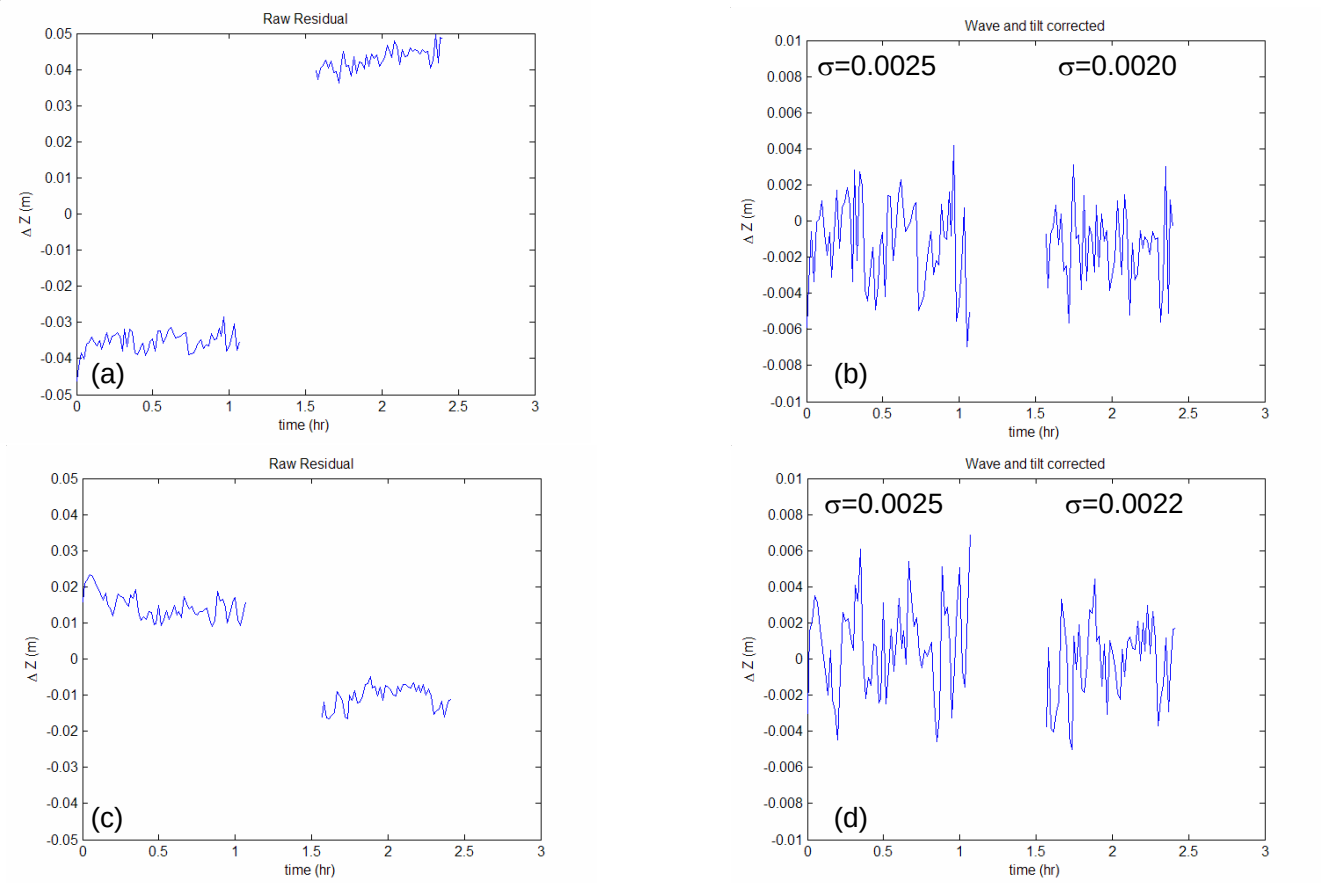

Figure 8: Double difference carrier phase residuals for MLA antennas. (a) raw data for AB baseline PRNs 27 & 31. (b) wave corrected for AB baseline PRNs 27 & 31. (c) raw data for CB baseline PRNs 27 & 31. (d) wave corrected for CB baseline PRNs 27 & 31.

MONITOR VALIDATION

After assessing the quality of the available measurements at the LGF, monitor implementation can be studied and its effectiveness evaluated. Two cases are shown in this section. The first one is a monitor for a Type A1 ephemeris threat. After a maneuver, the LGF needs to verify there is no anomaly in the broadcast ephemeris. As there is no previous validated ephemeris to compare with, this monitor is based on measurements. The second monitor is conceived to detect static Ionospheric fronts, as it has shown to be the most problematic case in previous work. [4]. In both cases, a simple test statistic is defined and a threshold is computed to meet the continuity, availability and integrity requirements of a system. The monitors will compare the test statistic generated for each case with this threshold, giving a pass/fail result. Finally ephemeris/iono anomalous errors are introduced to see if the results for each type of monitor agree with the analysis.

A1 EPHEMERIS THREAT MONITOR

When after a maneuver a satellite is flagged healthy by the GPS Control Segment, the LGF should not transmit corrections for that satellite to users before validating the new ephemeris. A waiting period of one day is assumed tolerable [5]. During that time, the LGF will collect measurements from that satellite, and from those measurements estimate a set of orbital parameters as input for the ICD-200 orbit model [2]. This estimate is obtained using a least squares fit. This whole process is described in detail in [1].

The positions from this measurement-generated ephemeris (x_{me}) are compared to the positions from the broadcast parameters (x):

$$\delta x = x - x_{me} \tag{6}$$

A test statistic S_e is obtained by normalizing this value:

$$S_e = \delta x^T \Sigma_{\delta x}^{-1} \delta x \tag{7}$$

The position error covariance is obtained at each point as:

$$\Sigma_{\delta x} = A_{(p,t)} \Sigma_p A_{(p,t)} \tag{8}$$

where: $A_{(p,t)}$ is the 3×15 sensitivity matrix of the position coordinates to the ephemeris parameters (a function of these parameters, and time) and,

Σ_p is the covariance of the estimated parameters.

The threshold needs to be defined next. Based on previous studies taking LAAS specifications as a reference, a conservative availability requirement (expressed as a fault free probability of false alarm) is:

$$P_{ffa} = 1.5 \times 10^{-4}$$

and the integrity requirement (expressed as a probability of misdetection) used is:

$$P_{MD} = 10^{-4}$$

The tightest threshold on a 3 DOF Chi Square test statistic that will comply with the P_{ffa} will be:

$$T_e = 4.501$$

The effectiveness of this type of monitor can be expressed by its Minimum Detectable Error (MDE), which describes the smallest error that will be detected by the monitor (with a certain probability of misdetection). Previous work [6] shows that an MDE smaller than 3500m is desirable, as it will not affect the current availability and continuity levels of the system.

The MDE of the monitor is given by the smallest non-centrality parameter on the Chi Square distribution λ that will have a probability of misdetection smaller than the specified, and the maximum eigenevalue of the position error covariance matrix:

$$MDE = \sqrt{\lambda} \max eig(\Sigma_{\delta x}) \quad (9)$$

Where $\sqrt{\lambda} = 8.053$ such that:

$$P_{MD} = P(S_e < T_e / \lambda) \quad (10)$$

Figure 9 shows two examples of the results obtained in the satellite position domain, and the corresponding MDE values for the same times. The position errors are shown for illustrative purposes.

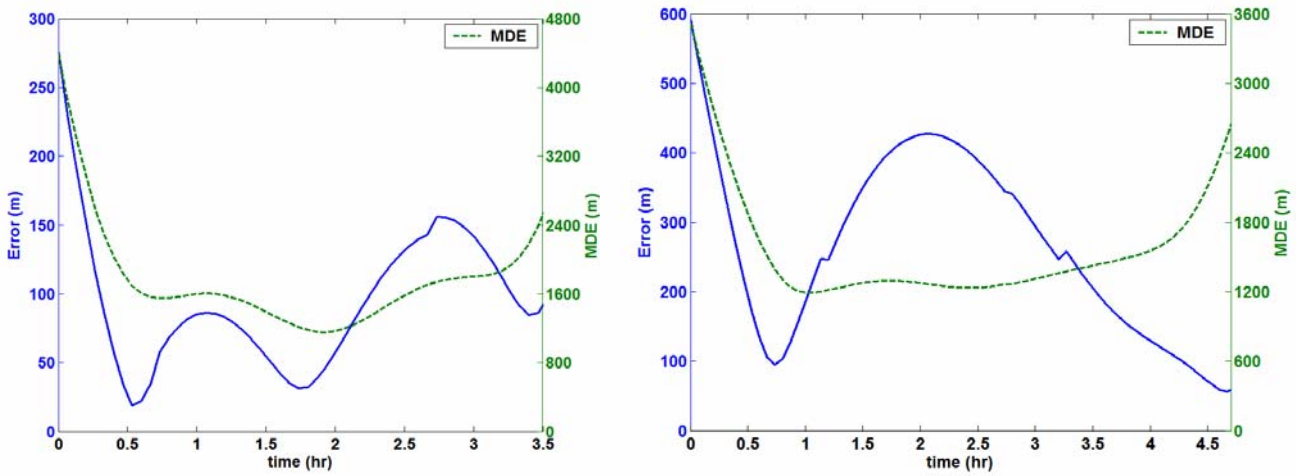

Figure 9: example of MDE values and satellite position error.

The numbers shown are somewhat higher than the ones obtained by covariance analysis in [1] where the maximum MDE values for a 100m baseline were close to 3500 m. This is due to the fact that the passes considered in this work are shorter (only HZA data was used), giving worse ephemeris parameter estimates. However, these results clearly support the claim of the previous covariance analysis [1][2], that baselines as short as 200 m are sufficient to monitor Type A1 threats. The final step to experimentally verify if the proposed monitor works, is to test it with real data. This was executed in two steps. First S_e values were computed with the fault free data to see if there were false alarms. Secondly, artificial errors were introduced in the ephemeris parameters to study the relation between misdetection and satellite position error magnitude.

Figure 10 shows an example of the fault free case for a satellite from rise to setting time. It can be observed there are no false alarms. For some isolated satellite passes the values of S_e were higher than the ones shown in the plot, (in one case reaching almost 4). Even though no false alarm was triggered, this might suggest some inflation is necessary to account for the non-perfectly gaussian distribution of the position errors (remember the spherical harmonics correction for the double difference measurements is only a good approximation).

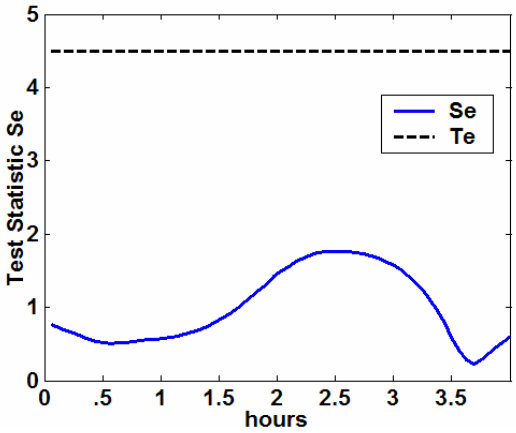

Figure 10: example test statistic values for fault free case.

To test the efficiency of the monitor in detecting failures, three different ephemerides are used:

- The broadcast ephemeris (considered to be the "true" ephemeris), used to compute satellite position x.
- The monitor estimated ephemeris, used to compute $\hat{x}$, and
- The failed ephemeris (obtained by adding an error to an ephemeris parameter one at a time) used to compute x_f.

The residual the monitor observes, and uses to compute S_e is:

$$\delta x = \hat{x} - x_f \tag{11}$$

The actual error in satellite position due to the failure is:

$$dx = x - x_f \tag{12}$$

Figure 11 shows the results using one satellite pass (S_e and T_e values were multiplied by 20 for plotting purposes). At each time in the pass errors were introduced for each ephemeris parameter as to produce position error magnitudes in the range of interest. The results for all epochs and all parameter failures were then sorted by the magnitude of dx. The MDE is also plotted, to visualize what the LGF is telling the users it can detect. Figure12 (detail of the lower left section of figure 11) shows that the maximum position error that went undetected was 622 m, which is significantly lower than the tolerable value for the MDE (3500 m). Note that for that particular point the MDE value is 2782m.

The final step of the experimental verification was taken successfully, and feasibility of the proposed A1 monitor is strongly backed up by the results.

IONOSPHERIC STORM MONITOR

The Ionospheric storm threat is particularly difficult to deal with. The threat itself is difficult to define, and as of today there is no monitor capable of detecting all possible hazardous shapes and sizes of a storm. To simplify its study the Iono storm is modeled as a gradient connecting two zones with constant phase advance. The details can be found in [4].

One of the most difficult cases is a static front, and in that regard, the baselines at the LGF could be of help in detecting it if a gradient exists between its antennas.

Consider the basic carrier phase measurement ϕ. A difference is taken between measurements from the two antennas forming each baseline to detect the ionospheric front. A double difference is then taken from a different satellite to remove the receiver clocks biases, and finally a triple difference is taken from a reference epoch to remove the cycle ambiguity. This measurement is defined as ϕ_{TD}. The standard deviation of this triple difference will be:

$$\sigma_{TD} = \sqrt{2}\sigma_{DD} \tag{13}$$

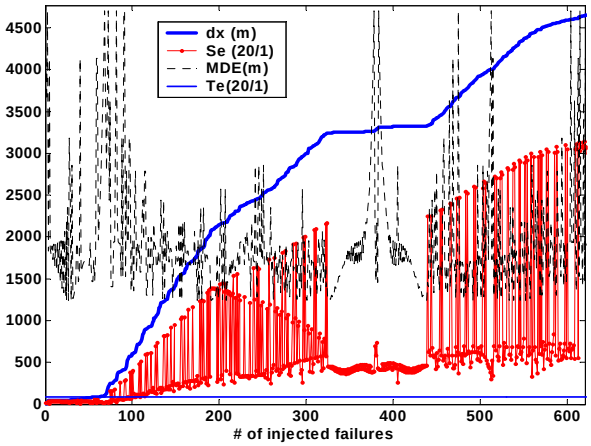

Figure 11: fault mode detection analysis.

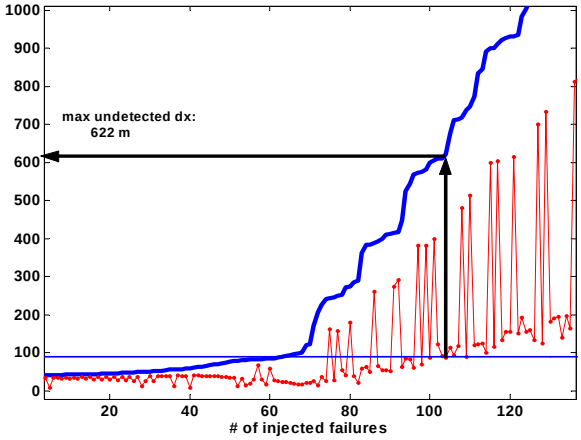

Figure 12: fault mode detection analysis (detail).

where σ_{DD} is the double difference standard deviation obtained in the previous section.

The difference from a second satellite can be taken because it is assumed that measurements to only one satellite will be affected by the front. That is based on the fact that, taking the maximum values for the front characteristics considered gives an Affected Sky Zone (ASZ) that is only a small part of the sky as seen from the LGF (at 350 km altitude), and a satellite far away from the satellite being monitored can always be found as to guarantee it is out of the ASZ.

The test statistic for this monitor will then be:

$$S_I = \frac{\phi_{TD} - \phi_C}{\sigma_{TD}} \qquad (14)$$

where ϕ_C is the computed triple difference using the broadcast ephemerides.

As the specifications for the ionospheric storm monitor have not been established, the P_{MD} and the P_{ffa} used for the A1 ephemeris monitor will be used as initial values.

The threshold of the monitor will then be: T_{iono}=3.791 (for a 1 DOF Chi square distribution).

Considering the linear model adopted for the ionospheric storm, the error introduced by the front can always be represented by a bias in the measurement from one antenna to one satellite, and thus will be a bias (b) in the triple difference measurement. Accordingly it will be also a simple bias in S_I, equivalent to $\frac{b}{\sigma_{TD}}$.

The effectiveness of this monitor can be measured by computing the Minimal Detectable Gradient (MDG) between antennas that will flag an alarm within the desired P_{MD}.

$$MDG = \sqrt{\lambda}\,\frac{\sigma_{TD}}{L} \qquad (15)$$

where L is the distance between the antennas.

To evaluate the effectiveness of such a monitor, different biases were introduced in the measurements of one antenna to see when S_I is bigger than $T_{iono.}$ The results show that for b>1.5 cm S_I is always bigger than the threshold. So the monitor can detect an Iono that produces 150mm/km bias or more in the carrier range measurements. Figure 13 shows 2 borderline cases of these results for biases of 12 cm and 15 cm respectively, were the bias is injected after rise time.

The gradients being studied at this moment range from 30 mm to 500 mm per km. Thus, in order to cover the whole range of threats, the baselines would have to be 500 m long.

The obvious flaw of this monitor is that if the storm was already in the ionosphere when the satellite rises, the bias will be eliminated when differencing, and it will go undetected.

A possible solution worth exploring is to take the reference measurement from the lapse in which the satellite is under the mask, or to elevate the mask if there is an Iono storm warning (from WAAS for example). The noise in the measurement will be worst, and the standard deviation of the triple difference measurement will be higher. As the satellite rises, the monitor's performance will improve until it reaches the one described before.

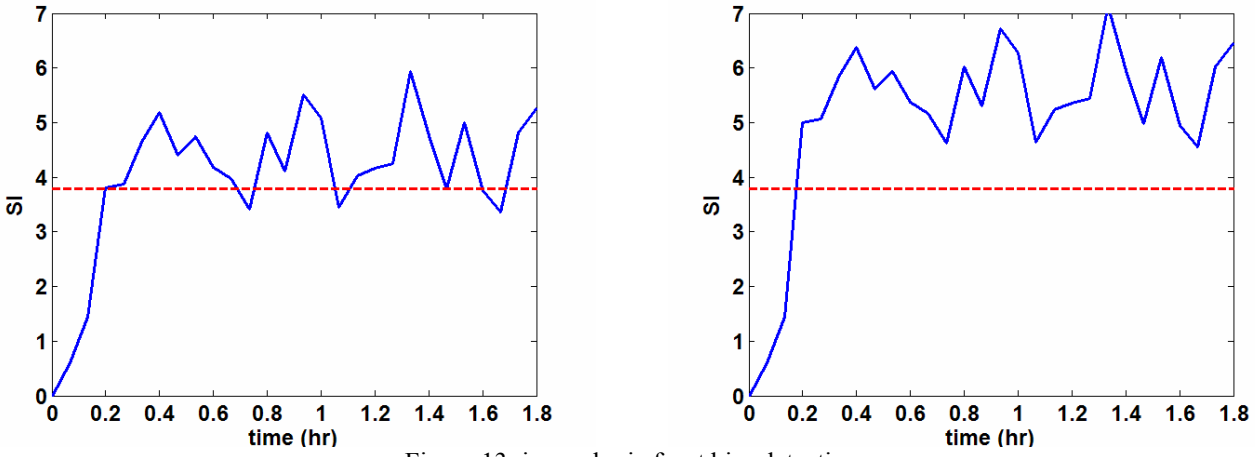

Figure 13: ionospheric front bias detection

Doing a conservative analysis, assuming the satellite rises in a direction perpendicular to the horizon, the distance the satellite signal's projection (at an ionosphere thin shell height of 350 km) travels before getting over the mask is bigger than 183 km (question mark in figure 14). So if its signal goes through a ionospheric front when the satellite becomes available for navigation, it is possible to find an unaffected reference measurement for all fronts that are smaller than that distance. If the mask is 7.5°, then the distance will be bigger than 280 km. However, the best standard deviation obtained to this moment for measurements below the 5° mask is larger than 10 mm. The minimal gradient detectable would be larger than 400 mm/km. This is still an option that requires some analysis, as in the presence of a ionospheric storm, the mask could be increased to give time for the monitor to validate a rising satellites measurements, the MDG will decrease with longer baselines, and the standard deviation of those measurements could be improved, as the spherical harmonics multipliers used in this work did not take into consideration measurements below the mask.

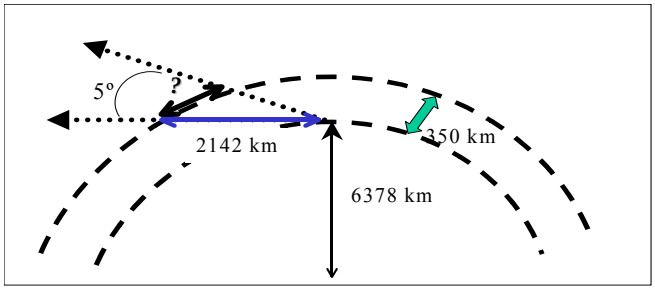

Figure 14: ASZ below mask analysis

CONCLUSIONS

The Local Area Augmentation System's Ground Facility has multiple high performance Integrated Multipath Limiting Antennas. Their behavior at the measurement millimeter level had not been studied before, as this was not necessary for previous applications. However, such degree of detail is needed to verify the performance of monitor applications like the type A1 ephemeris monitor. Big waves and non white noise patterns were found when plotting the measurement residuals over a day. It was determined that these were produced by phase variations between antennas. This undesirable effect was significantly reduced by applying spherical harmonics corrections for each baseline, reducing the standard deviation of the double difference measurement below 3 mm. With this quality of measurements MDE values similar to those predicted in the covariance analysis were obtained for the type A1 ephemeris monitor. To further extend the experimental verification, artificial errors were injected in the ephemeris broadcast and the maximum position errors that went undetected were quantified. They were comfortably below the MDE value for all cases. Finally some ideas were presented with respect to the static Ionospheric storm detection.

REFERENCES

1. Gratton, L; Pervan, B; Pullen, S; Orbit Ephemeris Monitors for Category I LAAS", *Proceeding of the IEEE Position, Location, and Navigation Symposium, PLANS '2004*, Monterey, CA, April 2004.

2. Gratton, L., "Orbit Ephemeris Monitors for Category I Local Area Augmentation of GPS" M.S. Thesis, Dept. Of Mechanical, Materials, and Aerospace Engineering, Illinois Institute of Technology, Chicago, July 2003.

3. Thornberg, D. B., et al., "LAAS Integrated Multipath Limiting Antenna", *Journal of the Institute of navigation*, Vol. 50, No. 2, Summer 2003, pp. 117-130.

4. Ming, L., Pullen, S., Walter, T., and Enge, P., "Ionosphere Spatial Gradient Threat for LAAS: Mitigation and Tolerable Threat Space", *Institute of Navigation's National Technical Meeting*, San Diego CA 2004.

5. Private conversation with Curtis Shively November 2003.

6. Shively, C. "LAAS Integrity Risk Due to Satellite Ephemeris Faults", *Proceedings of the 14th International Technical Meeting of the Satellite Division of the Institute of Navigation*, Salt Lake City, UT, September 11-14, 2001.